applied optics

Tunable laser frequency lock based on a temperature-dependent Fabry–Perot etalon

Yuan Jiang,[1,2] Xiateng Qin,[1,2] Dianqiang Su,[1,2] Zhonghua Ji,[1,2] Wenxin Peng,[3] and YanTing Zhao[1,2,*]

[1]State Key Laboratory of Quantum Optics and Quantum Optics Devices, Institute of Laser Spectroscopy, Shanxi University, Taiyuan 030006, China

[2]Collaborative Innovation Center of Extreme Optics, Shanxi University, Taiyuan, Shanxi 030006, China

[3]State Grid Chongqing Electric Power Research Institute, Chongqing 404100, China

*Corresponding author: zhaoyt@sxu.edu.cn

Received 4 April 2022; revised 24 May 2022; accepted 27 May 2022; posted 31 May 2022; published 13 June 2022

A simple method for laser frequency stabilizing by a temperature-tuned Fabry–Perot etalon is reported. The etalon is a plano–convex lens that permits tuning the length and refractive index via controlling the temperature for shifting wavelengths in the region of 852 nm, with a transmission spectral linewidth of ∼72.5 MHz and free spectral region of ∼16 GHz. Using this scheme, arbitrary frequency locking of a laser with an adjustable frequency resolution of 2.34 GHz/°C is realized, and MHz-level long-term stability is demonstrated. © 2022 Optica Publishing Group

https://doi.org/10.1364/AO.460238

1. INTRODUCTION

Laser frequency stabilization is critical in laser spectroscopy and atom physics, such as laser cooling and trapping [1–4], quantum manipulation [5], photon storage [6], and quantum teleportation [7,8]. In these experiments, the laser frequency needs to be stabilized in the desired range by feedback control, so the most important things are frequency stability and tuning flexibility. Several methods are commonly used for laser frequency locking. One is to lock the laser to an atomic or molecular resonance, often using a saturated absorption spectrum (SAS) to obtain a narrow linewidth and correspondingly better frequency stabilization [9]. This method has been widely used because of its simplicity, effectiveness, good stability, and reproducibility, but the disadvantage is that the laser frequency can be locked only on the inherent transition line, and the laser frequency range is limited. Alternatively, it is possible to use an external optical cavity to transfer the stability from a stabilized reference laser to the target laser, which has a significant difference in frequency [10]. For ultrastable lasers, the linewidth is usually narrowed to the order of sub-hertz or sub-millihertz with the help of the ULE cavity [11,12]. However, the primary disadvantages of these two technologies are high cost and complexity, which make them not suitable for a compact and straightforward experimental system.

A Fabry–Perot (F-P) etalon as a narrowband tunable filter has been widely studied during the past several years. Therefore, we hope to realize the continuous tunability of the locked laser within a wide range using a customized F-P etalon to build a low-cost and straightforward laser frequency locking system. Etalon frequency stabilization is a well-established technique. It is common to see lasers lock to a length-tuned [13] or tilt-tuned [14] etalon. Our scheme combines the intrinsic stability of the monolithic etalon with a wide free spectral region (FSR) and spatial mode filtering to customize plano–convex resonator construction. This special F-P etalon not only has the advantage of long-term stability and desirable suppression for unwanted modes [15], but also can lock the laser at any frequency within laser frequency coverage by tuning the cavity length.

In our experiment, we measured characteristic parameters of the etalon, studied the influencing factors of mode matching, frequency shift, and locking stability, verified the feasibility of arbitrary locking of the laser in a certain frequency range by temperature tuning, and analyzed the instability. It is very helpful to have laser locking without a reference line, such as strong coupling between the laser and microring resonator [16–19], and experiments in atom cooling and trapping. The frequency locking stability of the system can be further improved with the help of a lower thermo-optic coefficient etalon and a full PID servo [14,20,21].

2. EXPERIMENTAL SETUP

Figure 1 illustrates the experimental setup. The system is driven by an 852 nm diode laser (measurement laser). Part of the beam passes through the cesium (Cs) cell to obtain the SAS monitored by a photodetector (PD1). The other part of the beam passes through the etalon and then is detected by PD2, followed by feedback to lock the laser. The reference laser is locked to the

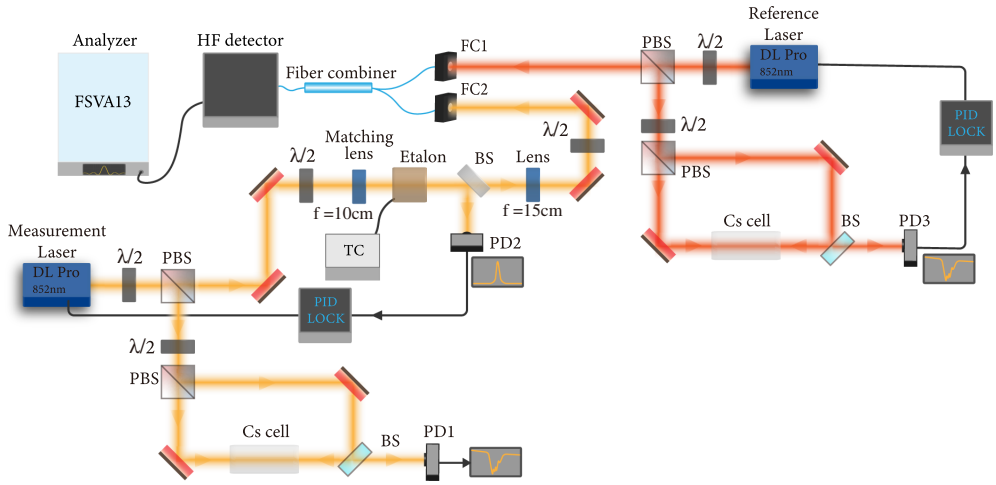

Fig. 1. Experimental Setup. λ/2, half-wave plate; PBS, polarization beam splitter; BS, beam splitter; PD1, PD2, and PD3, photodectectors; TC, temperature controller (connected to TEC of etalon); FC1 and FC2, fiber couplers; HF detector, high frequency detector; Analyzer, spectrum analyzer.

resonance transition peak of Cs atoms, providing a very stable reference frequency. The measurement laser and reference laser are coupled to fiber couplers FC1 and FC2, respectively. These two laser beams are combined using a fiber combiner and attenuated to a suitable level before entering the high frequency photodetector for beat-note measurement. The spectrum analyzer records the beat-note signal. The entire experimental device is enclosed to minimize the disturbance of airflow to the temperature of the etalon.

To have good mode matching, the mode in the cavity should satisfy two conditions. The first one is laser frequency matching, which is a standing wave condition and is often accomplished by tuning the laser current, temperature, PZT voltage or cavity length directly. The second one is a stable mode condition, which is accomplished by a mode matching lens to adjust the laser beam wavefront to match the curvature of the cavity reflection mirror. Using a lens with 100 mm focal length in our experiment for mode matching has a better suppression effect for an unwanted mode.

The F-P etalon we used is a solid plano–convex resonator constructed from a single substrate, and the design value of the high reflectivity coating on each surface is $R = 99\%$. BK7 was chosen as the substrate material with center thickness $L = 6.3$ mm, and curvature radius $r = 40.7$ mm, owing to its high transmission in the near infrared and high coefficient of thermal expansion, and satisfying the stability condition for plano–convex lenses: $0 < 1 - \frac{L}{r} < 1$. The quality of an etalon is governed by its finesse, which in the ideal case is

$$F_i = \frac{\pi\sqrt{R}}{1-R}. \tag{1}$$

The FSR of the etalon is given by the familiar formula

$$\mathrm{FSR} = \frac{c}{2nd\cos(\theta)}, \tag{2}$$

where c is the speed of light, n is the refractive index of the etalon, d is the etalon thickness, and θ is the angle of light propagation within the etalon relative to the surface. Normally θ does not change when mode matching is stable in an experiment. Thus the FSR can be tuned by altering n and d. For our temperature dependent etalon, changing the temperature will affect simultaneously both the cavity length and refractive index. According to the well-known resonant condition of the F-P etalon ($\nu = c/2n(T)d(T)$), the dependence of resonant frequency ν on temperature T can be written as

$$\frac{d\nu}{dT} = -\left(\alpha + \frac{1}{n_0}\frac{\partial n}{\partial T}\right)\nu_0. \tag{3}$$

The first term of Eq. (3) is the contribution of cavity length to the shift of resonant frequency as the temperature changes, and the second term is the contribution of the refractive index to the shift in frequency. Here $\partial n/\partial T$ is the temperature coefficient of refraction and can be obtained from the Sellmeier equation [22]

$$\frac{\partial n(\lambda, T)}{\partial T} = \frac{n_0^2 - 1}{2n_0}\left(D_0 + 2D_1\Delta T + 3D_2\Delta T^2 + \frac{E_0 + 2E_1\Delta T}{\lambda^2 - \lambda_0^2}\right), \tag{4}$$

where ΔT is the difference between T and T_0. D_0, D_1, D_2, E_0, E_1, λ_0 are constants that can be obtained from Ref. [23].

Thus the temperature stability will affect the frequency locking performance of the etalon. To reduce the influence of temperature drift on frequency locking as low as possible, we use a PID temperature controller (Thorlabs TED200C) to keep the temperature stable. According to Eq. (3), the cavity length and refractive index of the etalon can be tuned via the temperature control system to realize the frequency shift of the transmission peak and achieve arbitrary locking of laser frequency in a FSR.

3. EXPERIMENTAL RESULTS

PD2 provides the transmission spectrum across the etalon. The SAS of Cs is detected by PD1, which is used as a frequency standard to characterize the spectral properties of F-P etalons. As shown in Fig. 2(a), the transmission spectrum linewidth $\Delta\nu$

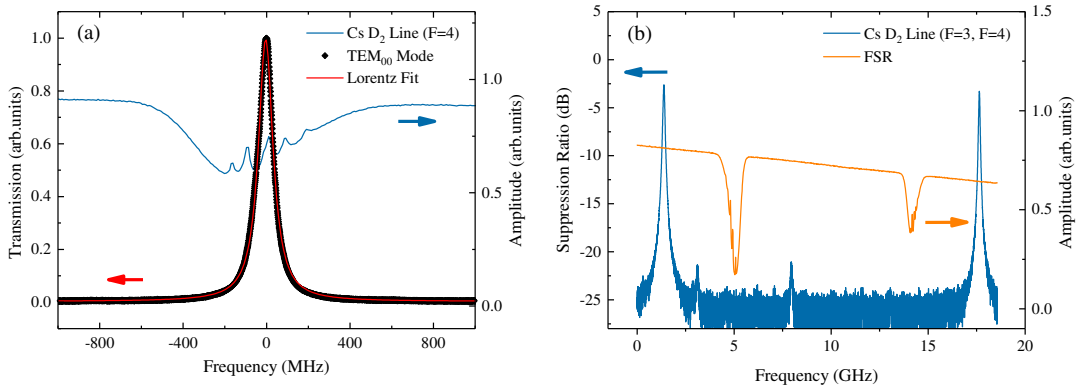

Fig. 2. (a) The blue line shows the SAS of cesium D_2 line transition of $6^2S_{1/2}(F=3) \leftrightarrow 6^2P_{3/2}(F'=2, 3, 4)$, which acts as a frequency ruler for the transmission spectrum (black points). The transmission peak represents the TEM_{00} mode, and the red line shows Lorentz fitting. (b) Measurement of free spectral region (FSR). The blue line shows the transmission profile over one full FSR. The orange line shows the SAS of cesium D_2 line transitions of $6^2S_{1/2}(F=4) \leftrightarrow 6^2P_{3/2}(F'=3, 4, 5)$ and $6^2S_{1/2}(F=3) \leftrightarrow 6^2P_{3/2}(F'=2, 3, 4)$.

of TEM_{00} mode is 72.5 MHz for a thickness of 6.3 mm etalon at 24°C. As shown in Fig. 2(b), the measured value of FSR is 16.256 GHz by continuously scanning the laser frequency across a range of 20 GHz, and the spectrum of the Cs D_2 line (F = 4 and F = 3) acts as a frequency ruler. The measured value is consistent with the expected value of 16.03 GHz in Eq. (2) at the same temperature.

According to $F = \mathrm{FSR}/\Delta\nu$, the actual measurement finesse is derived to be $F = 224$, which is less than the value of $F_i = 312$, expected according to Eq. (1). We believe that the loss is caused by the surface defect of the etalon, the imperfect matching of the wavefront with the surface, and the deviation of the real reflectivity coefficient from the design value. The suppression of unwanted modes is about 25 dB, as shown in the tiny peaks in the blue line in Fig. 2(b). By measuring the ratio of input and output optical power, it was found that the on-resonance transmission reaches 55%.

Equation (3) indicates that temperature changes can adjust the resonant frequency by affecting the refractive index and cavity length of the etalon. We recorded the shift in resonant frequency of one mode (transmission peak in Fig. 2) as a function of temperature, shown in Fig. 3. It shows that the frequency shifts linearly by 16 GHz from 21.94°C to 28.78°C, inducing a slope of $d\nu/dT \approx -2.34$ GHz/°C. Equation (3) allows us to obtain a theoretical value for $d\nu/dT$. Based on the data in Ref. [23], the thermal expansion coefficient α is 7.1×10^{-6}/°C for BK7 material. The refractive index of n_0 is 1.51 for this material under 852.1 nm, and the basic temperature is $T_0 = 20$°C. The resonant mode used here ν_0 is around 351.72 THz. For temperature tuning from 21.94°C to 28.78°C, the averaged $\partial n/\partial T \approx 1.34 \times 10^{-7}$/°C at wavelength (λ) 852.1 nm based on Eq. (4). Then $d\nu/dT \approx -2.48$ GHz/°C is derived according to Eq. (3), agreeing with our measured value of −2.34 GHz/°C in Fig. 3. We notice that the contribution of cavity length change to frequency tuning capability is greater than the refractive index change by two orders of magnitude. This demonstrates the availability of Eq. (3) and that the laser can be locked at any frequency in the range of 6.84°C.

With the help of the PID lock loop (shown in Fig. 1), the laser frequency can be locked to the transmission peak. To evaluate

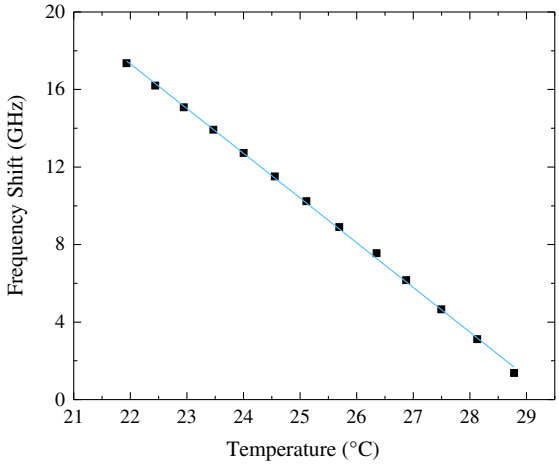

Fig. 3. Temperature tuning of laser frequency of one resonant mode. The black scattered points are the sampling point data, and the blue solid line is obtained by linear fitting of the data, with a slope of −2.34 GHz/°C.

the short-term behavior of lock loop stability, the error voltage signals were converted to frequency offset to provide accurate frequency deviation, as shown in Fig. 4(a). The frequency is locked to be within approximately ±1.1 MHz (blue line) with locking to the etalon, with a severe drift of more than 20 MHz (red line) in the same duration in the free-running status. This comparison shows that this system has a good short-term frequency stabilization effect.

To evaluate the laser frequency stability on the long-term scale, we use a high frequency photodetector and spectrum analyzer to measure the beat frequency with a stable reference laser, as shown in Fig. 4(b). The record shows a drift of ∼5 MHz during over 100 min. Figure 4(c) shows the Allan deviation of the recorded beat frequency and indicates that the long-term stability is below 1 MHz. The best stability is 0.15 MHz with an averaging time of 64 s.

A comparison of laser stability between short term and long term shows that the long-term frequency drift is severer, which

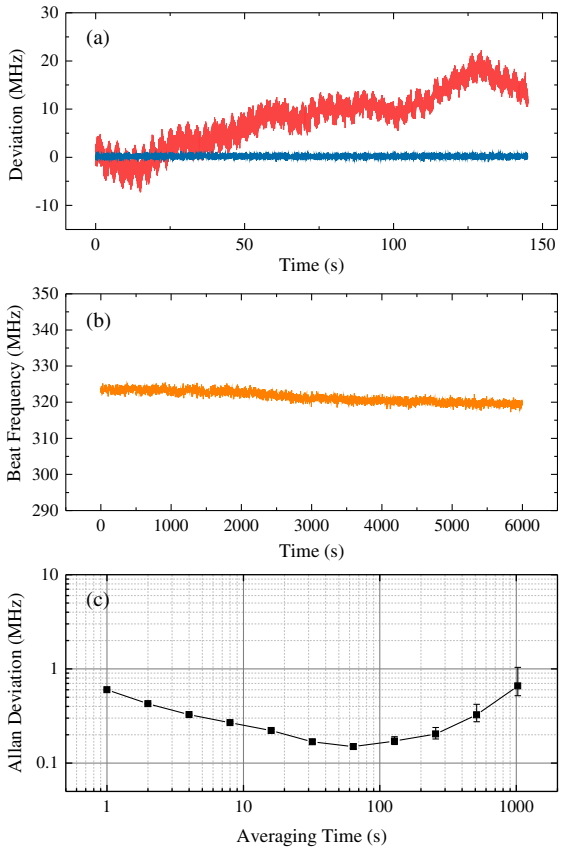

Fig. 4. Short-term and long-term stability of etalon resonance frequency. (a) Laser frequency stability in free-running (red line) and locked (blue line) status for 145 s. (b) Long-term beat-note measurement. (c) Allan deviation of the beat frequency data in (b).

is attributed to the temperature drift caused by the poor performance of temperature PID control, mechanical vibration, and laser polarization fluctuation. The influence of polarization on resonant frequency can be easily quantified by placing a half-wave plate in front of the matching lens. The result is shown in Fig. 5; with the polarization of the beam changing from s to p polarization, we find the frequency has a shift of ∼58 MHz and the amplitude has also changed. By replacing the half-wave plate with a glass plate, it was found that there was no apparent frequency shift or transmittance change when the glass plate was rotated.

Regarding the frequency shifts ($\delta\nu \approx 58$ MHz) of s and p polarization components, it is considered to be caused by the birefringence of the etalon [15], which has a subtle difference in the refractive indices for different polarized lights. According to the relationship between the resonant frequency and refractive index of the etalon, $|(d\nu/dn)| = \nu_0/n$, the refractive index difference $\delta n \approx 2.5 \times 10^{-7}$ can be derived. With regard to the amplitude change, we ensure that it arises from the difference of mode matching for s and p polarization lasers. As shown in Fig. 5, we found that if the laser polarization is rotated from s to p polarization, the amplitude of the dominant mode decreases but the side mode increases.

To assess the influence of polarization fluctuation on laser frequency shift under a stable experimental condition, we quantified this influence by monitoring the power of the s and p

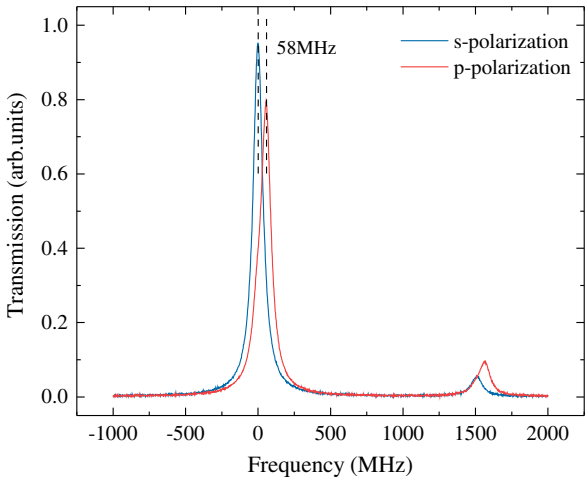

Fig. 5. Transmission profile of different polarizations through the 6.3 mm cavity showing a frequency separation of ∼58 MHz between the resonances for s and p polarizations.

polarization components of the laser before entering the etalon. In our measurement, s polarization is adjusted to have the maximum value and p has the minimum value. Their powers were measured simultaneously for a long time. The polarization fluctuation is derived by their ratio of approximately ±0.27%. As the maximum frequency shift caused by polarization rotation is about 58 MHz, shown in Fig. 5, it can be estimated that frequency fluctuation arising from polarization fluctuation is about ±157 kHz.

4. CONCLUSION

We have demonstrated a low-cost, simple laser frequency locking system using a temperature dependent F-P etalon. We measured the parameter characteristics of the F-P etalon and studied the frequency stability. As a good filter cavity, it has 25 dB suppression for unwanted modes while maintaining transmission of 55%. With the help of a temperature controller, the laser can be locked to the F-P etalon at any frequency with an adjustable frequency resolution of about 2.34 GHz/°C. The beat frequency measurement demonstrates a long-term frequency drift of about 5 MHz, and the long-term stability is characterized by an Allan deviation at MHz level. Tunability, a narrow linewidth, and wide FSR make the system a reliable tool, such as the coupling of microring resonators, laser frequency stabilization without a reference line, and so on. In addition, the stability of the locked laser could be further improved via more accurate temperature control, a more airtight insulation shell, and optimized locking circuit.

Funding. Science and Technology Project of State Grid (5700-202127198A-0-0-00).

Disclosures. The authors declare no conflicts of interest.

Data availability. Data underlying the results presented in this paper are not publicly available at this time but may be obtained from the authors upon reasonable request.

REFERENCES

1. S. Stenholm, "Laser cooling and trapping," Eur. J. Phys. **9**, 242–249 (1988).
2. E. S. Shuman, J. F. Barry, and D. DeMille, "Laser cooling of a diatomic molecule," Nature **467**, 820–823 (2010).
3. W. Ketterle and N. Druten, "Evaporative cooling of trapped atoms," Adv. At. Mol. Opt. Phys. **37**, 181–236 (1996).
4. M. Roghani, H.-P. Breuer, and H. Helm, "Modeling and control of entanglement dynamics in laser cooling of trapped atoms," Phys. Rev. A **85**, 012313 (2012).
5. P.-J. Tsai, Y.-F. Hsiao, and Y.-C. Chen, "Quantum storage and manipulation of heralded single photons in atomic memories based on electromagnetically induced transparency," Phys. Rev. Res. **2**, 033155 (2020).
6. M. T. Manzoni, M. Moreno-Cardoner, A. Asenjo-Garcia, J. V. Porto, A. V. Gorshkov, and D. E. Chang, "Optimization of photon storage fidelity in ordered atomic arrays," New J. Phys. **20**, 083048 (2018).
7. N. Lee, H. Benichi, Y. Takeno, S. Takeda, J. Webb, E. Huntington, and A. Furusawa, "Teleportation of nonclassical wave packets of light," Science **332**, 330–333 (2011).
8. L. Han, Y. Li, P. Xu, X. Tao, W. Luo, W. Cai, S. Liao, and C. Peng, "Integrated Fabry–Perot filter with wideband noise suppression for satellite-based daytime quantum key distribution," Appl. Opt. **61**, 812–817 (2022).
9. Y. Sun, F. Wei, Z. Dong, D. Chen, H. Cai, and R. Qu, "All-optical frequency stabilization and linewidth reduction of distributed feedback diode lasers by polarization rotated optical feedback," Opt. Express **22**, 15757–15762 (2014).
10. C. E. Liekhus-Schmaltz, R. Mantifel, M. Torabifard, I. B. Burgess, and J. D. D. Martin, "Injection-locked diode laser current modulation for Pound-Drever-Hall frequency stabilization using transfer cavities," J. Opt. Soc. Am. B **29**, 1394–1398 (2012).
11. S. Hirata, T. Akatsuka, Y. Ohtake, and A. Morinaga, "Sub-Hertz-linewidth diode laser stabilized to an ultralow-drift high-finesse optical cavity," Appl. Phys. Express **7**, 022705 (2014).
12. C. Wang, Z. Ji, T. Gong, D. Su, Y. Zhao, L. Xiao, and S. Jia, "A simple, low cost and robust method for measurement of the zero-crossing temperature of an ultralow expansion cavity," J. Phys. D **52**, 455104 (2019).
13. J. Lumeau, L. B. Glebov, and V. Smirnov, "Tunable narrowband filter based on a combination of Fabry-Perot etalon and volume Bragg grating," Opt. Lett. **31**, 2417–2419 (2006).
14. B. Gibson and B. McCall, "Tilt-tuned etalon locking for tunable laser stabilization," Opt. Lett. **40**, 2696–2698 (2015).
15. P. Palittapongarmpim, A. Macrae, and A. Lvovsky, "A monolithic filter cavity for experiments in quantum optics," Rev. Sci. Instrum. **83**, 066101 (2012).
16. H. Chandrahalim, S. C. Rand, and X. Fan, "Evanescent coupling between refillable ring resonators and laser-inscribed optical waveguides," Appl. Opt. **56**, 4750–4756 (2017).
17. A. C. Turner, M. A. Foster, A. L. Gaeta, and M. Lipson, "Ultra-low power parametric frequency conversion in a silicon microring resonator," Opt. Express **16**, 4881–4887 (2008).
18. R. Li, L. Zhou, J. Xie, A. Xie, and J. Chen, "Optimization of adiabatic microring resonators with few-mode and high-Q resonances," Appl. Opt. **54**, 10207–10212 (2015).
19. C. Fang, V. R. Shrestha, I. A. Ukaegbu, G. Ren, S. Pan, and B. Nakarmi, "Ultra-compact wideband filter with sidelobe suppression based on double modulated grating-assisted microring resonator," Opt. Contin. **1**, 623–632 (2022).
20. J. M. Kwolek, J. E. Wells, D. S. Goodman, and W. W. Smith, "Simple locking of infrared and ultraviolet diode lasers to a visible laser using a labview proportional-integral-derivative controller on a Fabry-Perot signal," Rev. Sci. Instrum. **87**, 055102 (2016).
21. M. Ghadimi, E. M. Bridge, J. Scarabel, S. Connell, K. Shimizu, E. Streed, and M. Lobino, "Multichannel optomechanical switch and locking system for wavemeters," Appl. Opt. **59**, 5136–5141 (2020).
22. M. Englert, P. Hartmann, and S. Reichel, "Optical glass: refractive index change with wavelength and temperature," Proc. SPIE **9131F**, 125–138 (2014).
23. SCHOTT, "Optical glass datasheet," SCHOTT Datasheets, 2021, https://www.schott.com/en-us/products/optical-glass-p1000267/downloads.